PAPER

Check for updates

Can blue-green infrastructure mitigate waterborne infection risks through recreational activities in densely urbanized waterways?

J. Petrucci, [iD] *[a] J. Derx, [iD] [ch] R. Sommer, [iD] [dh] J. F. Schijven, [iD] [e] H. Müller-Thomy, [iD] [fg] S. Dorner, [iD] [a] J. Jalbert [iD] [b] and F. Bichai [iD] [a]

Combined sewer overflows (CSOs) release pathogens into urban recreational water bodies and pose a threat to water quality, ecosystems, and public health. This risk is expected to increase with climate change, as more frequent and intense rainfall events are likely to exacerbate the number of overflows. Exposure to contaminants from CSOs can cause waterborne diseases, underscoring the need for effective stormwater management strategies. Blue-green infrastructure (BGI) offers a sustainable solution to mitigate the adverse impacts of CSOs while enhancing urban resilience through multiple co-benefits. This study combines hydrologic modeling with quantitative microbial risk assessment (QMRA) to assess the potential of BGI implementation strategies ranging from 0% to 50% of converted impervious surfaces, to mitigate the impacts of climate change on the microbiological quality and safety of urban rivers used for recreation downstream of CSOs. A strategy involving increased storage capacity by 28 000 m^3 was also considered to compare its performance in terms of risk reduction with BGI implementation. The approach was applied to an Austrian urban river catchment frequently used for recreational activities such as swimming, wading, and playing. Three planning horizons were analyzed – baseline (C20), near-term future (NTF) and long-term future (LTF). Results show that BGI reduces the probability of infection across all seasons, with the highest benefit observed in summer when recreational water use peaks. For *Cryptosporidium*, the 95th percentile infection risk in a worst-case scenario (*i.e.*, children swimming in the river) is reduced, when adding 50% of BGI, by 0.4 log$_{10}$ for the C20 period, 0.5 log$_{10}$ for the near-term future, and 0.6 log$_{10}$ for the long-term future, demonstrating the potential of BGI to improve the safety of recreational waters under changing climate.

Water impact

This study demonstrates how blue-green infrastructure (BGI) can reduce infection risks from combined sewer overflows in recreational urban water. By integrating hydrologic modeling with microbial risk assessment under climate change scenarios, it provides actionable evidence for sustainable stormwater management. The findings support BGI adoption to enhance urban water safety in a warming climate.

[a] Department of Civil, Geological, and Mining Engineering, Polytechnique Montreal, 2500 Chem. de Polytechnique, Montreal, Quebec QC H3T 1J4, Canada. E-mail: justine.petrucci@polymtl.ca

[b] Department of Mathematical and Industrial Engineering, Polytechnique Montreal, 2500 Chem. de Polytechnique, Montreal, Quebec QC H3T 1J4, Canada

[c] Institute of Hydraulic Engineering and Water Resource Management, TU Wien, Karlsplatz 13, 1040 Vienna, Austria

[d] Institute for Hygiene and Applied Immunology, Unit Water Hygiene, Medical University of Vienna, Vienna, Austria

[e] Environmental Hydrogeology Group, Geosciences, Utrecht University, Budapestlaan 4, 3584 CD Utrecht, The Netherlands

[f] Leichtweiß Institute for Hydraulic Engineering and Water Resources, Department of Hydrology and River Basin, Technische Universität Braunschweig, Germany

[g] Management, Technische Universität Braunschweig, Brunswick, Germany

[h] Interuniversity Cooperation Centre Water & Health, Vienna, Austria, https://www.waterandhealth.at

1 Introduction

Adequate urban water quality is critical for recreation, drinking water, and irrigation. Combined sewer overflows (CSOs) occur when the drainage system exceeds its capacity during rainfall or snowmelt events, discharging untreated wastewater into streams[1–3] posing significant public health risks.[4–7] At the European Union scale, the estimated annual volume of CSO was approximately 5.7×10^3 million cubic meters, highlighting the important impact of urban stormwater discharges on receiving water bodies.[8]

Climate change is expected to intensify precipitation, increasing the frequency of CSOs in North America and Europe by 2100, with the potential to release higher

concentrations of pathogens into urban waterways leading to public health concerns for recreational activities such as swimming.[9–11] Increased CSO frequency, combined with changes in pathogen loads, water temperature, and flow regimes, may exacerbate contamination downstream CSOs.[9,10,12–14] Derx, Müller-Thomy[9] projected CSO volumes to increase 21–53% by 2100 in Europe, intensifying public health risks.

Summer is a period when people are more inclined to enjoy water bodies for recreational activities: more people are swimming and for longer periods that could lead to an increased risk of exposure.[13] However, it is also the time when the number of CSOs can be the highest because of intense summer precipitation.[15,16] The impact of CSOs is more severe during this period, as in Europe, for example, it typically coincides with low flow regimes.[17,18] Swimming in unmonitored sites after CSOs can expose people to undetected pathogens, highlighting the need to ensure safe swimming water quality.

Access to waterways for recreation in urban areas provides multiple benefits enhancing citizens' quality of life and health.[19] With climate change increasing temperatures and heatwaves frequency by 2050, mitigating CSOs is crucial to protect swimming water quality and reduce health risks, as rising heat is expected to worsen morbidity and mortality across Europe.[20,21] Greening strategies can help reduce heat impacts and associated health risks.[22–25] While many cities are located near water, these blue spaces are often not fully integrated into urban planning, and their public health benefits are frequently overlooked by planning authorities.[26] Research has shown that water environments offer benefits for health and well-being by reducing heat stress, promoting physical activity, encouraging social interaction, and facilitating relaxation,[27–29] making safe access essential for both mental and physical health.

Blue-green infrastructure (BGI) offers a solution for urban water quality by promoting integrated stormwater management through infiltration and evapotranspiration.[30,31] BGI mitigates CSO impacts and microbial contamination by capturing and filtering runoff,[1,32,33] while also providing co-benefits such as reducing heat islands and improving urban environments.[31,34–38] By protecting recreational water areas, especially during hot summer months, BGI can help ensure safe and enjoyable spaces for aquatic activities.[13,39] To date it is unclear if how bioretentions affect recreational water safety in the receiving river water downstream CSO discharge.[40]

Quantitative microbial risk assessment (QMRA) is widely used to estimate health risks from waterborne pathogens, including those released during sewage overflows.[9,41–44] The QMRA method also allows comparing different management strategies.[41–43] European studies show measurable gastrointestinal illness (GI) risks from recreational exposure after rainfall and CSOs, with virus posing the highest risk.[9,41,44] Timm, Luther[44] estimated viral GI illness risks between 0.9% and 2.6%, and lower but non-negligible risks for *Cryptosporidium* (0.014%) and *Giardia* (0.0084%). Derx,

Müller-Thomy[9] projected up to 8% infection risk per exposure under future scenarios, highlighting the need for mitigation.

This study evaluates the effectiveness of BGI in reducing infection risks during recreational use of river water downstream of CSO discharges using QMRA modeling. While earlier studies examined BGI effects on pathogen loads from runoff or diffuse pollution,[45,46] its potential to reduce CSOs and ensure recreational water safety at urban swimming sites under climate change remains unexplored. Our approach integrates hydrological modeling with QMRA, extending the framework of Derx, Müller-Thomy[9] by incorporating BGI. Rainfall time series from regional climate models are downscaled to sub-daily scales and used in personal computer storm water management model (PCSWMM) to simulate CSO discharges, pathogen concentrations, and river flows under historical and future climate scenarios based on bias-corrected ÖKS15 projections.[47]

2 Method

Fig. 1 presents an overview of the methodology developed in this study.

The PCSWMM urban hydrological model simulated CSO discharges and pathogen concentrations, while a separate 1D river model accounted for upstream runoff and river flow. Combined microorganism data were used to calculate downstream infection risks across seasons (winter, spring, summer, autumn) and three planning horizons: reference (C20, 1971–2000), near-term future (NTF, 2021–2050), and long-term future (LTF, 2071–2100) following Derx, Müller-Thomy.[9] Bioretention was modeled from 0% to 50% in 5% increments, alongside a recently implemented storage measure at the study site. Bioretention are small depressions with a surface area determined by the drainage catchment, which capture some of the runoff from roofs, streets, and walkways.[30,31,48]

2.1 Study site description and data

The study area is a river catchment in Vienna, Austria, with a population of about 148 000 people. The river originates west of Vienna and receives inflows from several tributaries. It is primarily fed by runoff from urban and forested flysch areas. The sewer system is modeled using a PCSWMM sewer system sharing the same catchment area, proportions of land use and topographic gradients as the real study site, and real rainfall data from the study site. Fig. 2 shows a schematic representation of the studied area.

Although not officially a swimming site, the river is used year-round for recreation and serves during summer to refresh through activities like playing and wading.

2.2 Climate scenarios

For the climate impact analysis, we used the bias-corrected ÖKS15 projections,[47,49] based on regional climate models
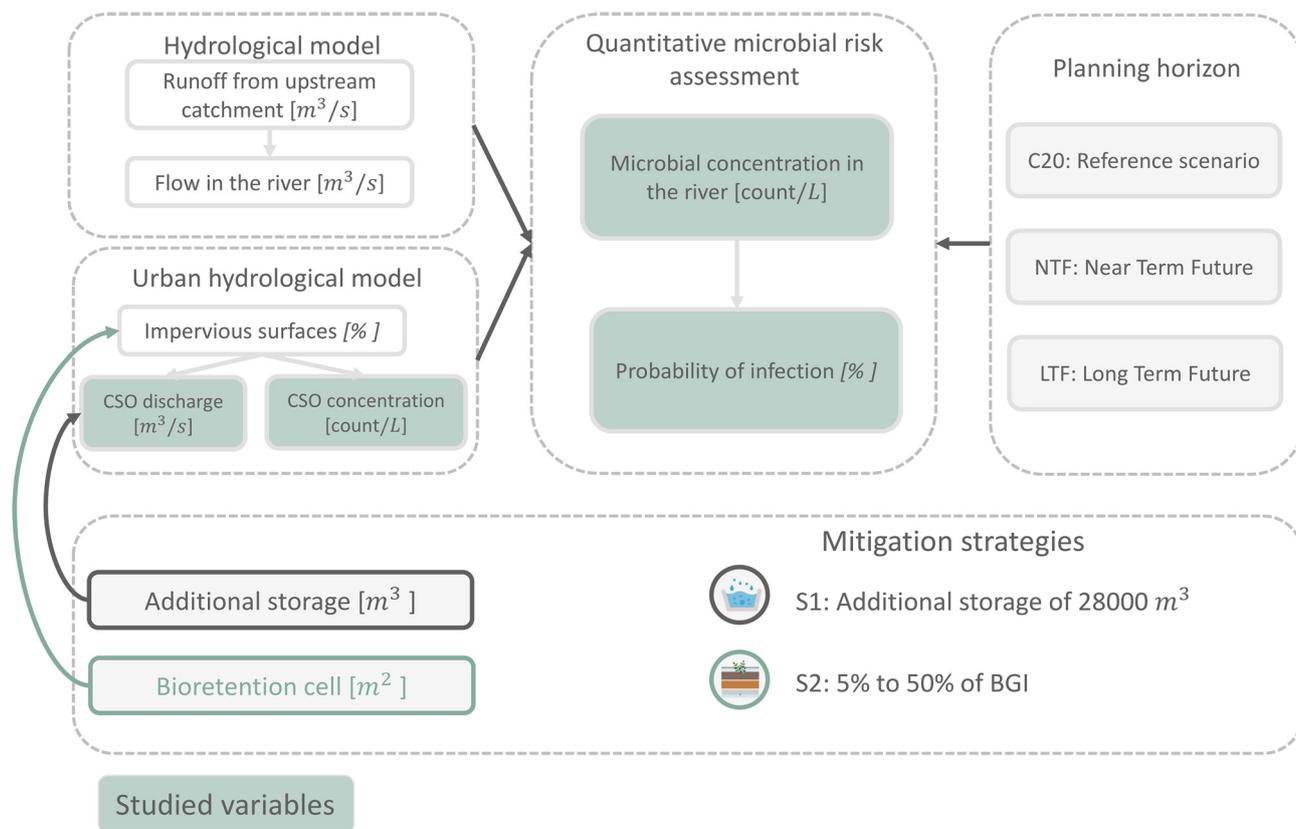
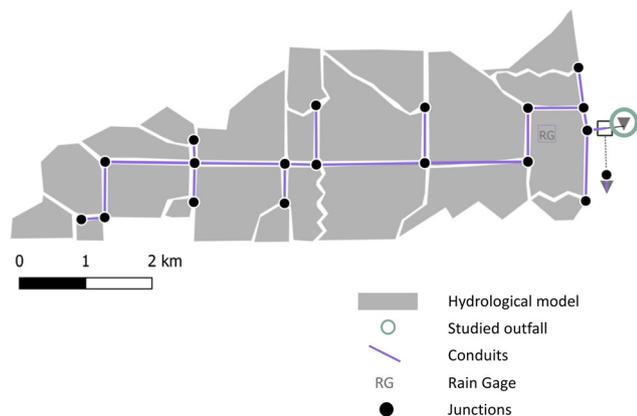Fig. 1 Conceptual diagram of the approach adopted in the study.

Fig. 2 Schematic study area with hydrological and urban hydrological model domain.

material for the complete list) which reflected the full range of possible increases in future infection risks (marked as coloured dots in Derx, Müller-Thomy,[9] Fig. 7). The study by Derx, Müller-Thomy[9] indicated that infection risk variability was greater across different seasons than across climate scenarios or rainfall disaggregation implementations. In total, thirty implementations of the disaggregated rainfall time series were applied for each planning horizon (C20, NTF, and LTF). For CMIP6 no regional climate model results were available for Austria when we conducted the study. However, although differences between climate periods C20, NTF and LTF are studied, the focus of the manuscript is on the impact on BGI and its effectiveness on reduction of infection risks. Using CMIP6 instead of CMIP5 would probably change the numbers of the results, the shown impact of BGI will remain the same – so the main message is still valid.

Disaggregated rainfall time series are used to increase the temporal resolution of climate-projected rainfall data, making them suitable for use in hydrological models. In this study, daily rainfall time series from the three selected climate scenarios were disaggregated to 5 minute intervals using the micro-canonical cascade model, selected for its proven performance in previous studies[51–53] as suggested in Derx, Müller-Thomy.[9] These disaggregated rainfall time series were then applied to the artificial sewer system model and the rainfall-runoff model.

(RCMs) from the EURO-CORDEX initiative, which in turn are based on global climate models (GCMs) from the CMIP5 framework.[50] ÖKS15 includes 13 GCM–RCM combinations for each of the RCP4.5 and RCP8.5 scenarios. Of the 26 total combinations, five were removed due to significant underestimation of rainfall in Eastern Austria (study region), and due to missing data.[47] This results in 21 GCM–RCM combinations that were applied in the study by Derx, Müller-Thomy.[9] For this study, from the 21 model runs, we selected three climate scenarios (C63, C73, C77, see SI S1

2.3 Artificial sewer system

To represent the urban drainage system, an artificial sewage system was used. This is a common approach for evaluating the impacts of rainfall datasets on CSO volumes when complete field data for modeling are lacking.[54] Moreover, artificial systems are often used to validate synthetic rainfall inputs as the one generated by the disaggregation.[55] The artificial sewage system used in this study, is adapted from Müller and Haberlandt,[54] and was modified to represent the hydrological characteristics of the study area to ensure the modeled and observed overflow events matched (see SI S2). The model is not an exact sewer network replica, but an artificial sewer network evaluated on monitored concentrations of enterococci, *Giardia* and *Cryptosporidium* in the river during 2018–2021 when CSOs and floods occurred.[9,54] Households in the model area connect to a combined sewer system meaning both runoff and sanitary water are in the same conduits. Sub-catchment widths were set based on actual dimensions, ranging from 400 to 3000 m, and surface slopes varied between 1.4% and 7.3%, with a mean of 4.1%, derived from a digital terrain model. The imperviousness was adjusted during calibration. It ranged from 50% to 100% (mean 81%), while conduit lengths ranged from 100 to 6000 m, totaling 31.3 km after calibration. A retention tank with a volume of 40 280 m^3 was included to store combined wastewater and stormwater when the treatment plant reaches capacity. Once exceeded, the overflow is discharged into the receiving water *via* CSOs. Microorganisms enter the sewer only *via* dry-weather flow C_{dry} [# L^{-1}]. All the initial parameters are adjusted as proposed in Derx, Müller-Thomy.[9] The parameters can be found in the SI S2. The urban hydrological simulations were run continuously to avoid any *a priori* assumptions about which rainfall extremes could trigger CSOs or the soil moisture conditions preceding rainfall events. This setup allows the model to realistically represent hydrological responses during intense rainfall events.

2.4 Rainfall-runoff model (HBV)

The runoff from the river catchment was simulated hourly using a distributed rainfall-runoff model.[56] The model domain area is 199 km^2, with a spatial resolution of 1 km × 1 km. The model was calibrated using hourly rainfall and temperature data, with parameters first assigned by hydrologic response units (HRUs) and then adjusted by comparing simulated and observed runoff (1990–2018; NSE = 0.51–0.93, overall NSE = 0.77; see SI S5 for details the training period is the first year (1990)). The calibrated model was then used to simulate the C20, NTF, and LTF planning horizons. Disaggregated rainfall time series were applied as spatially uniform input, with observed air temperature data from the Hohe Warte meteorological station during the C20 period.[9]

2.5 BGI implementation scenarios

Bioretention was modeled using the low impact development (LID) control editor in PCSWMM.[57–59] Selected for its small size suitable for densely built areas and its proven effectiveness in managing CSO quantity and quality, bioretention is among the most widely implemented LID practices.[1,32,60–62]

Bioretention design parameters and soil characteristics were derived from literature and case studies[1,32,58,63] due to the lack of site-specific data. This literature-based approach, commonly used in similar studies, enables evaluation of system performance within a local context. Bioretention systems consist of several layers. Precipitation and runoff infiltrate the soil and gravel layer, then exit *via* evaporation, further soil infiltration, underdrain flow to the sewer, or surface outflow redirected to the sewer. Detailed model configurations, parameter values (SI S3, Fig. S3-1) and details on the calculations for adjusting the parameters are provided in the SI S3.

Bioretention implementation strategies were based on the assumption that different percentages of impervious surfaces could be converted to bioretention, in a way that preserves the original surface functionality—for example, roads remain drivable and sidewalks remain accessible—while effectively reducing runoff.[31] Therefore, only a subset of the impervious surfaces was hydrologically connected to the bioretention systems. Specifically, only 30% of the impervious area was routed to the bioretention *via* runoff. The value of 30% represents an estimate of the fraction of impervious surfaces whose runoff can realistically be routed to bioretention systems, considering functional constraints such as drivable roads and accessible sidewalks (*vs.* water from roofs). It approximates the portion of runoff that can be treated, consistent with urban hydrology studies and design guidelines emphasizing a realist design rather than complete connectivity of impervious areas.[31,63,64] To assess the impact of bioretention implementation on infection probability, we incrementally added bioretention areas ranging from 5% to 50%, exceeding the threshold of 18% suggested by Furchtlehner, Lehner[65] in order to explore optimistic future scenarios for resilient cities. Although the MELCC[31] stormwater management guide recommends bioretention areas covering 5 to 10% of the impervious catchment area, the CSA W200:18 standard for designing bioretention systems suggests surfaces ranging from 10 to 20% of the impervious area of the watershed.[66] Thus, our study builds on these guidelines, extending the range of bioretention implementation even further to assess a broader spectrum of potential outcomes.

2.6 QMRA

The following sections details the QMRA modelling process of (1): identifying pathogens and their sources (hazard identification) (2); tracking their transport and fate to and within waterbodies, which can result in human exposure

when swimming (exposure assessment) (3); assessing pathogen infection risks through dose–response modeling and (4) characterising the risk by comparing the results to the health target.

The background concentration in the river and the ingested volume are represented by Gamma distributions to capture variability and quantify risk.[9,67,68] For both parameters, we consider a random value from the gamma distribution for each time step of 1 hour. In this study, we adapted a derived program coded in Python from Schijven, Derx[68] to perform the QMRA.

2.6.1 Hazard identification. In this case study, a hazardous situation arises from heavy rainfall causing a CSO, leading to a high concentration of pathogenic microorganisms in a swimming area. Enterococci serve as an indicator of fecal contamination.[69,70] Their elevated levels in freshwater or marine environments suggest the presence of fecal matter and, consequently, the potential occurrence of pathogenic microorganisms originating from fecal sources.[69] In addition, two reference pathogens were used, *Cryptosporidium* and *Giardia*, since they are protozoa that significantly contribute to waterborne disease outbreaks.[71] In Canada, in the United States and in Europe, *Giardia* is the most frequently reported protozoan in water for recreation.[72–74] *Giardia* and *Cryptosporidium* are also reference pathogens identified by the USEPA.[42] The concentration in the river (C_{river}) after a CSO is calculated as described in eqn (1):

$$C_{river} = \frac{C_{CSO} \cdot Q_{CSO}}{Q_{river}} + C_{river,bg \cdot obs} \quad (1)$$

where C_{river} [count per l] is the microbial concentration in river water, C_{CSO} [count per l] is the simulated microbial concentration in the CSO discharge, Q_{CSO} [m^3 s^{-1}] in the simulated CSO discharge, Q_{river} [m^3 s^{-1}] is the river discharge and $C_{river,bg \cdot obs}$ [count per l] is the microbial background concentration in river water. C_{CSO} and Q_{CSO} are obtained through PCSWMM simulation (section 2.2). Q_{river} is obtained from the rainfall runoff model (section 2.3) and $C_{river,bg \cdot obs}$ is an estimation of the background concentration of *Cryptosporidium*, *Giardia* or enterococci. The background concentration of *Giardia* is modeled using a Gamma distribution with parameters (0.3, 1.2), resulting in a mean of 0.36 cysts per l (SI S4, Table S4-1). Similarly, *Cryptosporidium* follows a Gamma distribution with parameters (0.6, 0.9) and a mean of 0.54 oocysts per l, while enterococci is modeled with parameters (0.27, 1500, 6) and a mean of 405 particles per l (SI S4, Table S4-1). The enterococci concentration was estimated from the *E. coli* concentrations obtained through the PCSWMM model by multiplying the *E. coli* values by a factor of 0.278 (ref. 69, 75 and 76) which was the ratio of the mean concentrations of enterococci and *E. coli* observed in raw wastewater by Derx, Müller-Thomy.[9] The Gamma distribution is appropriate for this context, as it effectively models non-zero background concentrations and ensures positive values.

2.6.2 Exposure assessment. Exposure assessment evaluates the likelihood of ingesting pathogens during recreational activities, with swallowed water volume depending on activity type, duration, and age. For this risk assessment, the dose (D) is calculated based on the pathogen concentration in the river and the Gamma-distributed volume (V, in liters) of water swallowed per person per swimming event: men ($r = 0.45$, $\lambda = 60$), women ($r = 0.51$, $\lambda = 35$), and children ($r = 0.64$, $\lambda = 58$) and the respective averages of 27 ml, 17.85 ml and 37.12 ml.[67,68] Here, r is the shape parameter and λ the scale parameter of the Gamma distribution. The expected swallowed volume is calculated as $r \times \lambda$. A lower r means a more skewed distribution, capturing the variability in ingestion volumes across the population. The scale parameter λ stretches or compresses the distribution, affecting the average volume and variability of water ingested while swimming. In this study, we considered children as the worst-case scenario.

The risks of infection per person and exposure event are calculated assuming that recreation takes place directly downstream of the sewage emission. The ingested dose (D) during recreational use is calculated with eqn (2):

$$D = C_{river} \times V \quad (2)$$

where D is the ingested dose, C_{river} is the concentration in the river calculated with eqn (1) and V [m^3] is the swallowed volume during a swimming event depending on the type of swimmer (men, women, children).

Note that the time elapsed between the end of the overflow event and swimming was not explicitly considered. The probability of infection at an hourly resolution was calculated and then the risk was averaged over the entire season or year (more information can be found in the SI section S8, Fig. S8-1). To reflect seasonal variations in exposure probability, infection risks were weighted by seasonal factors: 0.01 for winter, 0.1 for spring and autumn, and 1 for summer.[9] The seasonal factor is at its lowest in winter and moderate in spring and autumn since people are least inclined to go swimming during those seasons but can practice other activities and can be exposed to contaminated water by playing, or when walking dogs taking baths in the river. While a more detailed approach using survey-based exposure data—such as that employed by Sterk, de Man[13]—could have been used, we opted for this simplified method to avoid introducing additional complexity that could mask the effects of climate change and of the addition of bioretention. Alternatively, exposure could be modeled more realistically based on periods when recreational water contact is more likely to happen. For example, during warmer months or when water temperatures exceed a certain threshold.

2.6.3 Dose–response. To calculate the risk of infection per person and exposure event, we used dose–response models. For *Cryptosporidium* the risk of infection (P_{inf}) was calculated using the hypergeometric dose–response model:

Paper

$$P_{\text{inf,}Cryptosporidium}(D) = 1 - {_1}F_1(\alpha, \alpha + \beta, D) \qquad (3)$$

where P_{inf} is the probability of infection per swimming event, α is 0.3, β is 1.1 and ${_1}F_1$ is the confluent hypergeometric function[77] and D is calculated with eqn (2).

For *Giardia* the exponential dose–response model was used with $r = 0.02$:[78]

$$P_{\text{inf,}Giardia}(D) = 1 - e^{-rD} \qquad (4)$$

where P_{inf} is the probability of infection per swimming event and D is calculated with eqn (2).

Eregno, Tryland[41] found that the probability of infection is highest on the first day following a rainfall event, decreases on the second day, and then declines more gradually up to the third day. This suggests that pathogens remain present in surface waters for an extended period after a CSO event. While few people are likely to swim during rainfall itself, recreational activities often resume within hours or days following the event—at a time when exposure risk may still be high. Our study accounts for this by evaluating infection probabilities on an hourly basis over a 30 year period, capturing both short-term and long-term exposure patterns. This approach also allows assessing cumulative risks over a full swimming season,[42] which is relevant for informing public health recommendations. Furthermore, while regulated beaches may have closure protocols, many people swim in informal or unmonitored locations, where no such guidelines exist.

2.6.4 Risk characterization. The final step of the QMRA process involved calculating the concentrations of enterococci, *Cryptosporidium*, and *Giardia* in the swimming site, as well as the risks of infection per person and exposure event (*Cryptosporidium*, and *Giardia*). These calculations were

done at hourly intervals under climate change conditions, both with and without the implementation of BGI.

3 Results

3.1 Hydrological model results

For the results of the urban hydrological model, we categorized CSO events into three ranges based on the discharge flow rate: <1.0 m³ s⁻¹ (low range), 1.0–1.5 m³ s⁻¹ (medium range), and >1.5 m³ s⁻¹ (high range). Fig. 3 shows, on the one hand, the variation in overflow volume with the effects of climate change and, on the other hand, the effects of adding BGI for the three planning horizons (C20, NTF, LTF) and for four implementation strategies. Fig. 3 also shows the variability between the three selected climate scenario (C63, C73, C77).

Fig. 3 shows the fraction of 5 min time steps with CSOs for the three defined categories. The fraction of time steps with CSO increases in the future (NTF, LTF) compared to the reference period C20, with a more pronounced increase observed under the LTF than the NTF, and for larger CSOs (greater than 1.5 m³ s⁻¹). For the strategy without BGI, compared to the C20 planning horizon, we found that for CSO < 1.0 m³ s⁻¹, the number of time steps increased by 10% for the NTF planning horizon and by 15% for the LTF planning horizon. For medium CSOs (1.0 < discharge rate > 1.5 m³ s⁻¹), the fraction of time steps with CSO in the NTF and the LTF respectively increase by 14% and 30%. For CSO > 1.5 m³ s⁻¹, the fraction of time steps with CSO increases by 25% (NTF) and 53% (LTF). These changes are consistent across all BGI scenario implementations (SI S6, Fig. S6-1). In the climate scenario C77 (SI S6, Fig. S6-1) we observed a significant increase (95% to 227%) in the fraction of simulation 5 min time steps during which CSO occur
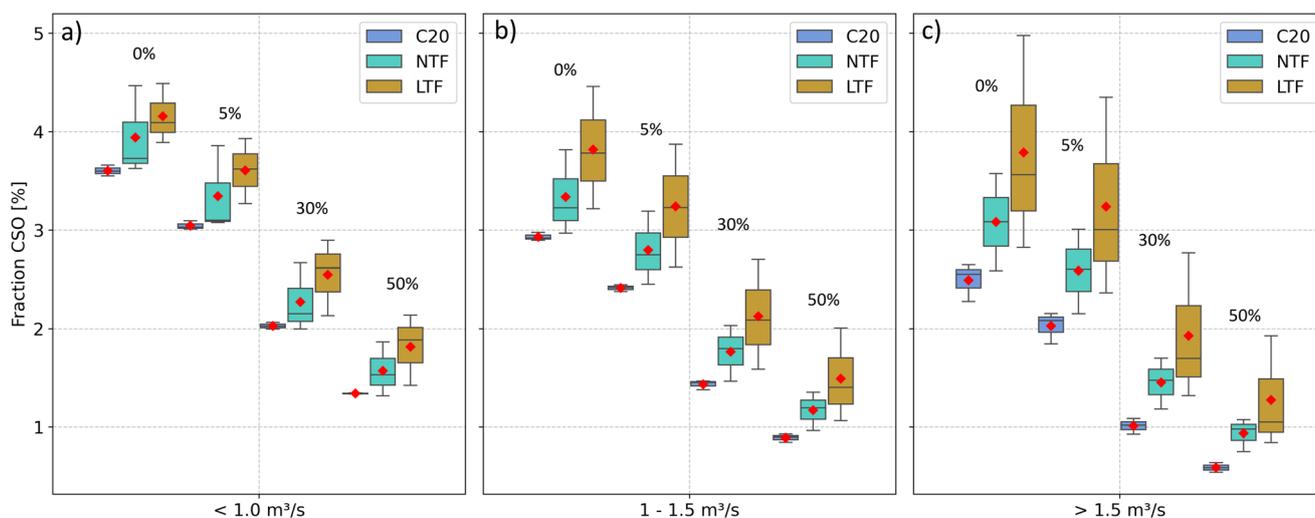

Fig. 3 Fraction of simulation 5 min time steps with CSOs [%] for the C20, NTF and LTF (*y*-axis) for different percentages of BGI (0%, 5%, 30%, 50%) implementation. CSOs are differentiated for discharges of (a) <1.0 m³ s⁻¹, (b) 1–1.5 m³ s⁻¹ and (c) >1.5 m³ s⁻¹. Red diamonds show the mean, boxes the 25th and 75th percentiles, whiskers the 5th and 95th percentile, and black horizontal lines the median values (results are for all the climate scenarios). C20 (blue) in the reference period, NTF (turquoise) is the near-term future period and LTF (brown) is the long-term future period.

especially for medium and large CSO flowrates (1–1.5 m³ s⁻¹ and >1.5 m³ s⁻¹). The increase in the fraction of time steps likely indicates a rise in total overflow volume. A higher fraction of time steps means that CSOs are active for longer durations, implying greater water discharge. This effect is more pronounced for large CSO events (>1.5 m³ s⁻¹), where the relative increase is nearly three times larger compared to small events (<1.0 m³ s⁻¹). Although the fraction of time steps does not directly quantify overflow volume, the combination of longer CSO duration and higher discharge rates strongly suggests an overall increase in overflow volumes.

Results show that the implementation of BGI is effective to reduce CSOs duration under current and future climate conditions (Fig. 3). These results are also consistent across the three tested climate scenarios. The data demonstrate that the implementation of BGI has a more significant effect on larger overflows (>1.5 m³ s⁻¹), with reductions in volumes reaching up to 76% with the highest BGI implementation strategy (SI S6, Table S6-1). For example, in the case of CSOs >1.5 m³ s⁻¹, without BGI, the fraction of time steps with CSO is 2.28, but with 50% BGI, it can be reduced to 0.54 (SI S6, Table S6-1). In contrast, the impact of BGI is less pronounced for smaller overflows (<1.0 m³ s⁻¹), where the maximum reduction is 63% in the same planning horizon (C20). However, the impact of BGI is attenuated by climate change, with reductions being less significant in the LTF scenario compared to the C20 scenario. For instance, in the LTF scenario, for CSOs >1.5 m³ s⁻¹, the maximum reduction with 50% BGI is 71%, compared to 76% in the C20 planning horizon (SI S3, Table S3-1). Indeed, the effectiveness of BGI decreases with rising temperatures and extreme climatic events, suggesting that additional adaptive management strategies will be required to maintain these benefits over the long term and mitigate the effects of overflows under future climate change scenarios. These results highlight that increasing levels of

BGI implementation (from 0% to 50%) leads to greater CSO volume reduction, particularly for larger events. The implementation of BGI at 30% is projected to significantly reduce the frequency of future CSOs compared to scenarios with C20 and no BGI implementation.

Table 1 shows statistics of CSOs, river flows and mixing ratios during all seasons with and without BGI implementation for the three periods (reference period C20, NTF and LTF).

According to the results, the river runoff [m³ s⁻¹] is highest in spring, and lowest in autumn in all periods (Table 1). The mean annual river runoff increases relative to C20 by 8 to 20% under the NTF and the LTF. In comparison to C20, the river runoff increases from 4 to 20% for the NTF, and from 12 to 35% for the LTF over different seasons. The mean mixing ratio between CSO and river discharges (Q_{cso}/Q_{river}) shows an increase under both the NTF and the LTF scenarios relative to C20, indicating a stronger increase of CSO discharges than in river runoff. Across all seasons, CSO flows increase during both the NTF and the LTF periods compared to the C20 baseline.

When comparing the strategy without BGI and with a 50% level of BGI implementation, CSO discharges decrease by 59% to 76%, and the mixing ratio decreases from 70% to 86% for both future planning horizon (NTF, LTF) over different seasons. Changes in river flow due to BGI are presumably small and were thus not considered in the rainfall-runoff model.

3.2 Microbial river water quality and infection risks during recreational use

Without BGI, the dilution of microorganisms in river water results in mean concentrations of *Cryptosporidium* at 3.91 oocysts per L, *Giardia* at 31.65 cysts per L, and enterococci at 1.54×10^5 CFU L⁻¹ downstream of CSO discharges under the C20 scenario, across all seasons (SI S7, Fig. S7-1),

Table 1 Mean values of CSO discharge rates, river flows and mixing ratios over the complete simulation time without BGI and with 50%-BGI implementation (climate scenario no C73)

| Scenario | Season | River runoff [m³ s⁻¹] | 0% | | 50% | |
			Q_{cso} [m³ s⁻¹]	Mixing ratio	Q_{cso} [m³ s⁻¹]	Mixing ratio
C20	Yearly average	2.08	0.12	0.03	0.03	0.01
	Winter	2.00	0.11	0.05	0.03	0.01
	Spring	2.93	0.12	0.02	0.04	<0.01
	Summer	2.11	0.13	0.03	0.04	0.01
	Autumn	1.27	0.11	0.04	0.03	0.01
NTF	Yearly average	2.25	0.15	0.04	0.05	0.01
	Winter	2.15	0.14	0.07	0.05	0.02
	Spring	3.04	0.16	0.03	0.07	0.01
	Summer	2.54	0.20	0.04	0.07	0.01
	Autumn	1.27	0.09	0.03	0.02	<0.01
LTF	Yearly average	2.49	0.17	0.04	0.06	0.01
	Winter	2.69	0.17	0.07	0.06	0.02
	Spring	3.34	0.19	0.03	0.08	0.01
	Summer	2.51	0.19	0.04	0.06	0.01
	Autumn	1.42	0.13	0.05	0.04	0.01
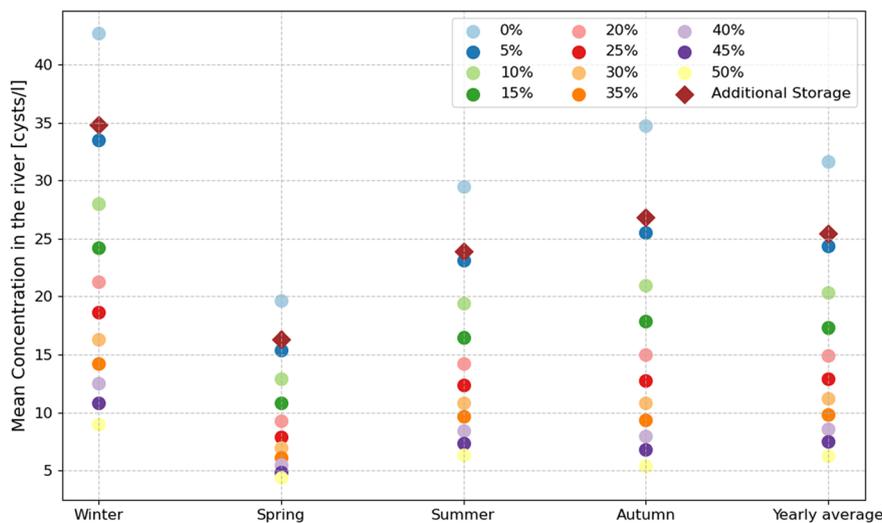
Fig. 4 Mean concentration of *Giardia* [cysts per l] for the climate scenario no C73 per season. The mean concentration in river water is calculated over 30 years of simulation time for the C20 (NTF and LTF periods results are in the SI S7, Fig. S7-1).

highlighting the effectiveness of BGI in improving water quality.

The highest concentrations occur during winter, which may be explained by the fact that river flow is generally at its
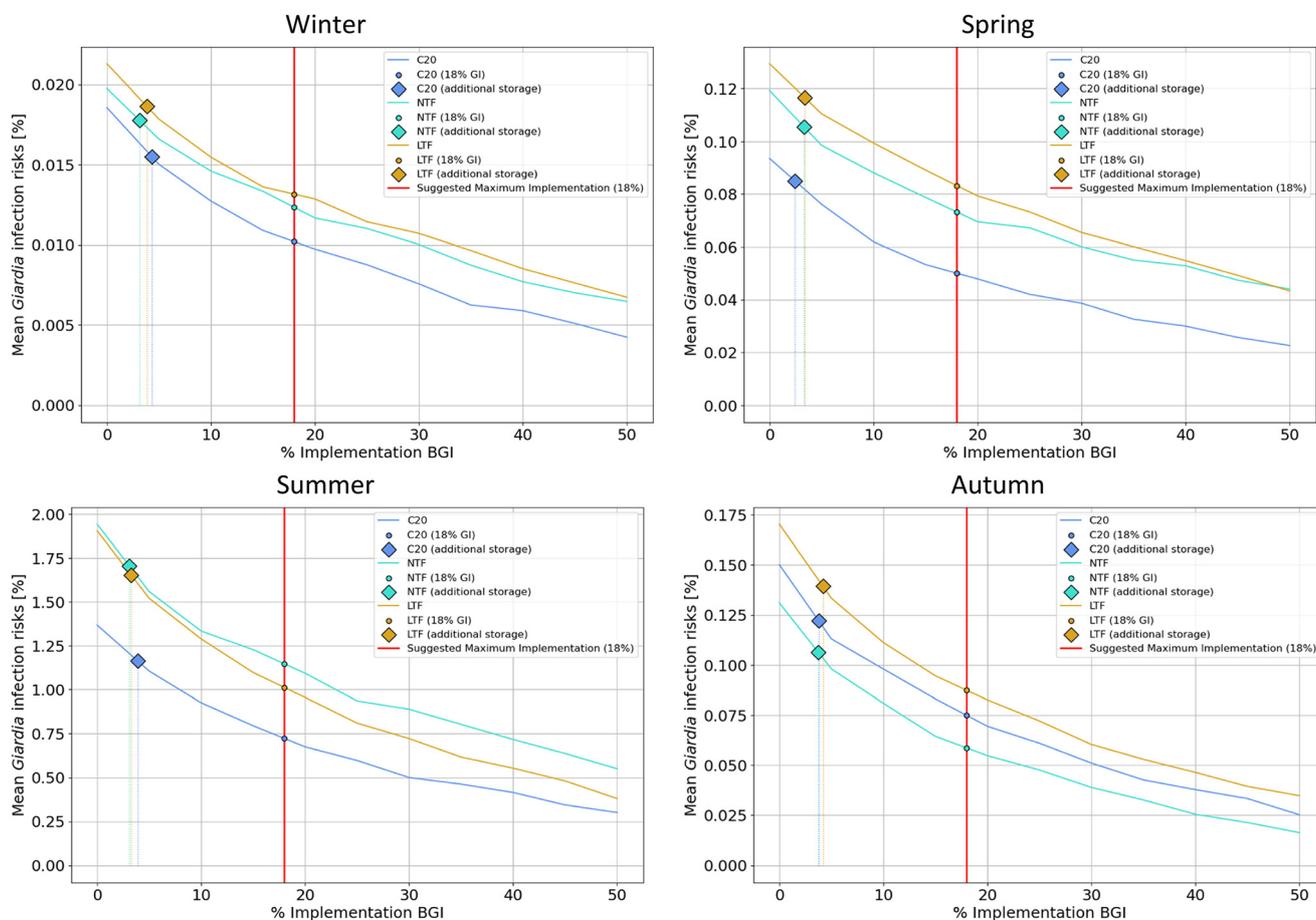

Fig. 5 Mean *Giardia* infection risks [%] per person and exposure event during recreational use of river water calculated over 30 years of simulation time for the C20, NTF and LTF periods as function of BGI implementation (continuous lines). Diamonds represent the probability of infection when additional storage is added, and for the corresponding percentage of BGI required to achieve the same reduction in infection risk. Red line and dots represent the maximum suggested implementation. Note that the scale of the *y* axis is different for each season.

lowest during this period, while background concentrations is stable across seasons. Results also indicate that overflow volumes tend to be higher in winter, likely due to reduced infiltration rates during colder months, which further affects flow and pollutant loading dynamics.[63,79] Without accounting for snow accumulation, runoff is estimated to be higher and infiltration lower (Gougeon *et al.*, 2023 (ref. 63)). Since snowpack processes are not explicitly simulated, PCSWMM likely overestimates winter runoff by treating precipitation as direct rainfall rather than snow accumulating on the ground. Consequently, runoff (and overflow volumes) may be overestimated in winter and underestimated during the spring snowmelt period, potentially influencing the modeled overflow volumes and seasonal patterns.

During the C20 period, concentrations with 50% BGI implementation are reduced by 0.74 log (81%) for enterococci, 0.53 log (71%) for *Cryptosporidium*, and 0.72 log (81%) for *Giardia* compared to 0% BGI. For the planning horizon C20 we observed that the greatest reductions are in in autumn (Fig. 4) and the same applied for NTF and LTF planning horizon (results not shown, SI S7, Fig. S7-1). However, as the percentage of BGI increases, the additional reduction in concentration becomes less significant. This diminishing effect highlights the saturation point of treatment potential: BGI are primarily implemented on impervious surfaces like roads and parking lots. Once a substantial portion of these target areas is equipped with bioretention systems, the remaining surfaces either already

Table 2 Percentage of change in the mean infection risk [%] by season by time period without BGI (0%) and with 50% BGI implementation and the effectiveness of the measure in reducing infection risks in % and $\log_{10}$ units. Higher reduction is green and lower reduction is red

	Season	Scenario	Infection risks [%]		Effectiveness of measure in reducing infection risks	
			0% BGI	50% BGI	Reduction (%)	$\log_{10}$ reduction
Giardia	Winter	C20	0.017	0.004	77	0.630
		NTF	0.018	0.005	75	0.611
		LTF	0.018	0.005	73	0.581
	Spring	C20	0.091	0.022	75	0.610
		NTF	0.104	0.034	68	0.497
		LTF	0.111	0.035	69	0.513
	Summer	C20	1.409	0.286	80	0.693
		NTF	1.732	0.448	75	0.606
		LTF	2.015	0.544	75	0.614
	Autumn	C20	0.156	0.027	83	0.770
		NTF	0.169	0.033	81	0.736
		LTF	0.206	0.058	73	0.587
Cryptosporidium	Winter	C20	0.017	0.007	59	0.389
		NTF	0.019	0.008	59	0.386
		LTF	0.019	0.008	57	0.370
	Spring	C20	0.117	0.059	49	0.295
		NTF	0.127	0.067	48	0.281
		LTF	0.134	0.069	48	0.287
	Summer	C20	1.553	0.639	59	0.386
		NTF	1.786	0.783	56	0.360
		LTF	2.038	0.853	58	0.383
	Autumn	C20	0.166	0.063	62	0.423
		NTF	0.179	0.068	62	0.421
		LTF	0.206	0.087	58	0.383

support natural infiltration or contribute minimally to runoff. As a result, further expansion of BGI yields diminishing returns, since the main sources of contaminated runoff have already been addressed. Additionally, bioretention systems only treat runoff from ground-level impervious surfaces (*e.g.*, streets and parking lots), and not from rooftops. Consequently, they capture only a portion of the total runoff from both impervious and permeable surfaces. In PCSWMM, this phenomenon is modeled by specifying which surfaces are subject to treatment (see section 2.4). The point at which diminishing returns become evident varies based on the microorganism, climate period, and season, typically occurring between 20% and 40% BGI implementation. The results under all the climate scenarios and for enterococci and *Cryptosporidium* can be found in the SI S7, Fig. S7-1.

We calculated the probability of infection per person and exposure event during recreational use of river water as a function of BGI implementation percentage (ranging from 0% to 50%) for two reference pathogens, *Giardia* and *Cryptosporidium*, across all seasons (Fig. 5, Table 2). Since the parameter enterococci is a fecal indicator, we did not calculate the probability of infection.

Fig. 5 shows the relationship between BGI implementation percentage and mean infection risk per person per exposure event. We found a non-linear decreasing trend. The most substantial reductions in infection risk occur with the initial increments of BGI, while additional implementation leads to gradually smaller improvements. This reflects a pattern of diminishing returns, as shown in Fig. 5, and highlights the strategic value of prioritizing BGI implementation in high-risk areas to maximize public health benefits. Fig. 5 also shows that only around 3% of BGI implementation is needed to reach the same reduction in the probability of infection as is obtained with an additional storage of $28\,000$ m^3. Results

for all three tested climate scenarios (see section 2.3) can be found in the SI (S7, Fig. S7-2). All results follow the same trend: the infection risk decreases with the implementation of BGI over the three simulated periods.

For both reference pathogens, the highest variation is observed during autumn for the NTF period. There is less variation observed during winter and spring, indicating that the impact of BGI is less significant during these two seasons. This is because the soil remains frozen in winter and becomes saturated with water in spring from snowmelt, leading to reduced infiltration during these periods[63,80] and on the contrary in warm seasons, low flows can limit dilution effects leading to higher infection risks.[81] Across all periods, the effect of BGI is significant, with reductions ranging from 69% to 91% (0.67 to 1.02 log). To confirm that the reduction is statistically significant, we used the two-proportion *Z*-test. This statistical method assesses whether the difference between the proportions of two groups is significant. A *Z*-value greater than 1.96 indicates statistical significance at the 5% level. In our analysis, all reductions were statistically significant, with *Z*-values ranging from 3 to 47.

To investigate the upper percentile of the infection risk, we evaluated the cumulative probabilities for *Cryptosporidium* and *Giardia* during the C20, NTF and LTF periods without BGI and with the highest BGI implementation (50%) (Fig. 6).

Fig. 6 demonstrates the effectiveness of bioretention implementation. The 95th percentile infection risks range from 0.09% in winter to 6.51% per person and exposure event in summer for C20 and increase by 0.1–0.2 log$_{10}$ in the future for *Cryptosporidium*. The 95th percentile infection risks range from 0.07% in winter to 4.62% per person and exposure event in summer for C20 and increase by 0.2–0.3 log$_{10}$ in the future for *Giardia*. During all seasons, we observe a decrease in probability of infection with the addition of
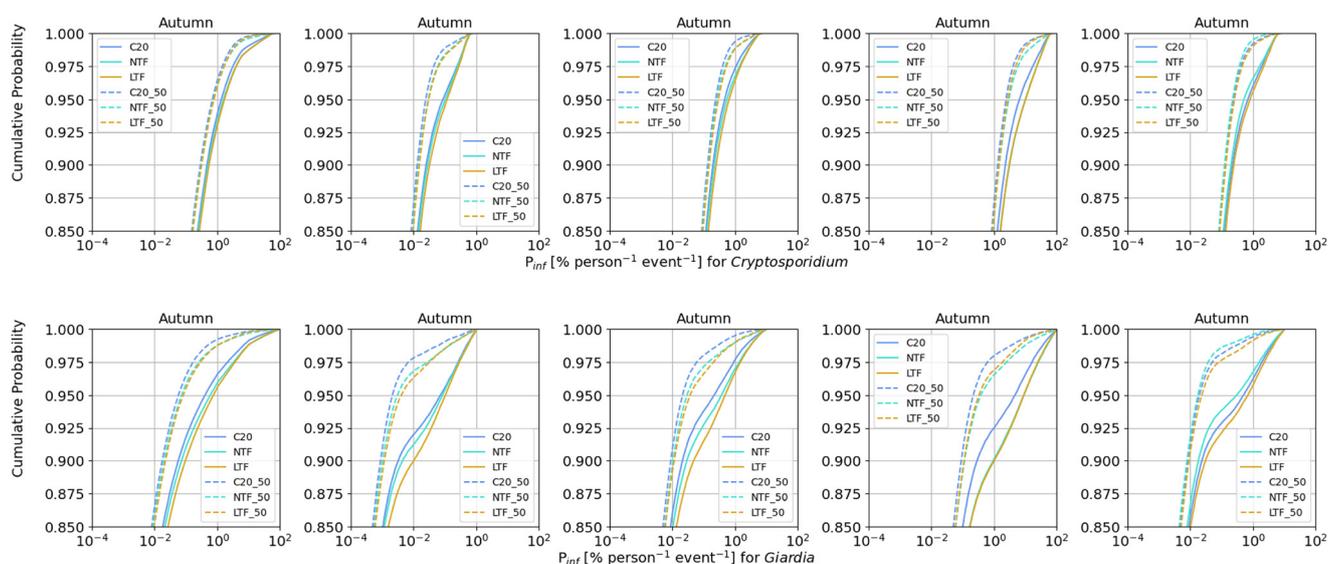

Fig. 6 Cumulative probability distributions of the 95th *r* percentile infection risks [% per person and exposure event] for *Cryptosporidium* and *Giardia* during recreational use in the river downstream of sewage emissions from CSOs over 30 years of simulation time for the C20, NTF and LTF for the climate scenario no C73 (full lines: no BGI, dotted lines: 50% BGI implementation).

BGI. For example, in the summer, *i.e.*, when people are most likely to swim and practice recreational water activities, the reduction in probability of infection for *Cryptosporidium* for the C20, NTF and LTF periods are $0.4 \log_{10}$, $0.5 \log_{10}$ and $0.6 \log_{10}$ respectively (all the results can be found in the SI S7, Fig. S7-3). The impact of BGI seems more pronounced for *Giardia* than for *Cryptosporidium*. This difference may be explained by several factors, including differences in pathogen behavior and environmental persistence, and removal efficiency in bioretention systems.[72,82] The greater effectiveness of BGI for *Giardia* compared to *Cryptosporidium* may be explained by differences in their physical and hydrological behavior. *Giardia* cysts are larger than *Cryptosporidium* oocysts, making them more likely to be removed through physical filtration in porous media like bioretention systems.[82] *Cryptosporidium*, on the other hand, is more resistant to drying and can remain suspended in water for longer periods, reducing the effectiveness of physical removal processes such as sedimentation and infiltration. In the case of our study, this difference can be explained by the fact that the *Giardia* concentration is initially higher in the sanitary water, due to the modeling in PCSWMM (SI S2, Table S2-2).

4 Discussion

4.1 Integrating BGI in climate change adaptation

This study presents a novel probabilistic–deterministic model to assess climate change impacts and the effectiveness of BGI in improving microbiological river water quality and recreational safety downstream of CSOs. For the first time, it addresses whether BGI can reduce infection risk for swimmers, highlighting its potential for urban water management and co-benefits.

BGI systems are effective for urban water management, but also to provide various co-benefits, such as maintaining aquatic and terrestrial habitats, and reducing heat islands.[31,37,83] BGI also has a positive impact on the quality of a community's living environment. This type of landscaping contributes to health and well-being.[84] The introduction of BGI can help reduce the health risks associated with swimming due to CSOs discharge, but also further improve the overall health of communities through promoting an active lifestyle and reducing heat islands, although such benefits can be more difficult to assess quantitatively. Disability-adjusted life years (DALY) could also be estimated for these additional health co-benefits in urban communities, which could enable a fairer comparison between the costs and benefits of BGIs *versus* grey infrastructure.

Combined sewer overflows (CSOs) are major contributors to degraded urban water quality, leading to habitat deterioration, higher drinking water treatment costs, and reduced recreational value.[85,86] Reducing CSOs would bring many benefits for the community including health, environmental, economic and social benefits.[87–91] First, as demonstrated in this paper, a reduction in CSOs can reduce the probability of infection for swimmers downstream from CSO structures, providing safe recreational water for the population. Eregno, Tryland[41] reported gastrointestinal illness risks from 0.06–1.6% for *Giardia* and 0.4–1.8% for *Cryptosporidium*, consistent with our current estimates of 1.4% and 1.6%, respectively—values within the WHO's acceptable range (WHO, 2003). Under future climate conditions (LTF), the risk rises to 2% for *Giardia* and *Cryptosporidium*, exceeding the WHO target (19 cases per 1000 swimmers), indicating a potential public health concern in the context of climate change. Given the projected rise in gastrointestinal illness risk under future climate, BGI represents a proactive, long-term strategy to reduce contamination at the source. It complements traditional public health measures and helps maintain acceptable recreational water quality.

Furthermore, although CSOs may represent a small fraction of the total annual wastewater discharge, they contribute disproportionately—between 30% and 95%—to the annual load of various pollutants.[87,88] Thus, reducing CSOs can enhance water quality and protect aquatic ecosystems.[17] The results show a significant reduction in CSO volumes when adding BGI infrastructure (Fig. 3). The reduction ranges from 16% to 76% for C20, 15% to 68% for NTF, and 11% to 71% for LTF. The greater the implementation of BGI, the larger the reduction in CSO volumes. These findings are consistent with previous studies that have highlighted the effectiveness of BGIs in controlling overflows.[1,32,92,93] For instance, Autixier, Mailhot[32] found that CSO volume reductions with bioretention cells ranged from 13% to 62%. Other studies that used a variety of BGI types showed that CSO volume attenuation could range from 50% to 99%, depending on the deployment strategy and the specific mechanisms of each technology.[1,94]

Our results show that implementing BGI can mitigate climate change impacts by reducing CSO volumes, consistent with previous studies.[94] However, its effectiveness diminishes under future conditions: in the LTF planning horizon, CSO ($>1.5 \text{ m}^3 \text{ s}^{-1}$) reductions reach 71% with 50% BGI, compared to 76% in the C20 planning horizon. Similar performance reductions due to climate change have been reported for bioretention[95–98] Climate change will induce an increase in rainfall as reported by Haslinger, Breinl[99] which will alter the water balance in bioretention systems, highlighting the need to update design standards Spraakman, Martel.[100] Our results show higher precipitation across all seasons and planning horizons (C20, NTF, LTF), consistent with projections for Central Europe[101,102] and observed increases of 8–22% for NTF and 15–33% for LTF in high-intensity, long-duration events,[9] which correspond with the observed increase in CSO discharge. While BGI can reduce CSO volumes, their runoff retention capacity may decline under future rainfall intensity–duration–frequency shifts and higher soil saturation, underscoring the need for adaptive designs.[98] Such strategies include increasing soil layer depth, storage

layer depth, or the surface area of bioretention cells,[103,104] integrating hybrid gray-green systems, or using real-time control technologies to optimize retention.[98,105,106] Plant selection can further enhance hydrologic services and system resilience.[107] Together, these adaptive approaches provide a framework to maintain the risk-reduction benefits of BGI in urban rivers under evolving climate scenarios.

The method developed in this study can also be applied to evaluate microbiological water quality by analyzing simulated concentrations of fecal indicators in the river. In our study area, the simulated mean concentrations of enterococci (SI S7, Fig. S7-1) correspond to microbiological water quality category D, indicating a greater than 10% risk of gastrointestinal illness (GI) according to WHO guidelines for recreational water quality.[70] However, the implementation of 50% BGI improves water quality to category C, reducing the GI risk to 5–10%, thereby demonstrating the positive impact of BGI on water quality. This reduction in GI risk is expected to translate into a proportional decrease in the burden of disease expressed as disability-adjusted life years (DALYs), as demonstrated in Timm, Luther[44] who identified a relationship between microbial water quality categories, GI incidence, and associated DALYs in recreational water environments. The DALY concept provides a complementary tool to the QMRA for evaluating and comparing health risks arising from a specific environment for a specific population and behaviour and for comparing with other health risks of daily life.[44]

The results highlight significant benefits of BGI for water quality but show that effectiveness per converted impervious surface declines beyond 20–40% coverage. Beyond this threshold, additional improvements are marginal, suggesting that further expansion may be less efficient. Interestingly, Ghodsi, Zahmatkesh[108] found that implementing BGI—including bioretention cells, vegetative swales, infiltration trenches, and permeable pavement—on less than 1% of the catchment surface still reduced runoff volumes by approximately 14% under various climate change scenarios. This highlights the potential for small-scale but strategically placed BGI interventions to achieve measurable impact. Together, these findings are valuable for decision-makers aiming to maximize water quality benefits while optimizing resources and minimizing spatial and financial limits.

4.2 Study limitations

Despite these promising outcomes, certain limitations of the study must be acknowledged. The approach presented in this paper can be applied to other urban river settings by using site-specific historical rainfall time series with high temporal resolution and regional climate models. However, in the developed method, BGI was not implemented following a strategic plan; rather, the same percentage of implementation was applied uniformly across all urban catchments. In practice, BGI is often deployed opportunistically rather than strategically, leading to

inefficient resource allocation and limiting benefits.[109,110] To maximize effectiveness, a more strategic approach is recommended. Planning tools such as the spatial suitability analysis tool (SSANTO) that consider multiple objectives and stakeholder preferences can help identify the most strategic locations for BGI.[110,111] For example, studies using the SSANTO tool to design BGI implementation strategies showed that distributing BGI to achieve target rates of impervious surface conversion—while prioritizing areas with higher suitability scores and allocating fewer interventions in lower-suitability zones—can enhance bioretention performance and maximize sector-specific resilience, highlighting the benefits of strategic, context-sensitive implementation.[112,113] Future applications should integrate such prioritization methods alongside a calibrated urban hydrological model to optimize BGI placement and maximize its effectiveness.

The current method does not incorporate snowmelt into the urban hydrological model, unlike the study by Gougeon, Bouattour[63] conducted in Quebec, where snow is a significant factor impacting runoff and the occurrence of CSOs. Although cold climates are not directly addressed in this study, future research and planning should consider winter conditions. Snowfall events, snow accumulation, and snowmelt must be taken into account to more accurately estimate the full potential of bioretention systems during snowy periods, when snow can significantly affect runoff.[63] Yet, for infection risk assessments through recreational uses, colder periods are generally less relevant due to a lower likelihood of exposure, as fewer people swim in cold weather.

This study focused on bioretention as a representative type of BGI due to their widespread use[62] and well-documented hydraulic and pollutant removal performance.[32,94,114] While this choice limits direct comparison with other BGI types as suggested in Joshi, Paulo Leitão,[1] the methodology developed here is adaptable and could be applied to assess other BGI solutions such as green roofs by adjusting key model parameters (e.g., retention capacity, infiltration rate, contributing area). While this study uses a simplified bioretention cell representation to estimate the performance of BGI, we acknowledge that individual system performance can vary widely depending on site-specific conditions such as soil type, maintenance, and design. As such, results at the catchment scale should be interpreted as indicative rather than predictive. Further studies incorporating spatial heterogeneity and real-world implementation constraints would help refine these projections.

In this study, we worked with the CMIP5 framework because for CMIP6 no regional climate model results were available for Austria when we conducted the study. While CMIP6 models exhibit higher spatial resolution and improved representation of climate processes compared to CMIP5 models,[115] the impact of using CMIP5 is unlikely to significantly alter the conclusions regarding BGI's impact on mitigating the infection risks, as both CMIP5 and CMIP6

ensembles indicate similar increases in precipitation and streamflow, with comparable spatial variability.[116] Recent studies concluded that projected changes in mean annual precipitation and hydrological response are broadly consistent between CMIP5 and CMIP6 (ref. 116 and 117) uncertainty in QMRA model inputs—such as microbial concentrations, treatment efficiency, and environmental conditions—can significantly impact risk estimates and overall model outputs.[118,119] Uncertainty increases during extreme events like heavy precipitation, affecting pathogen levels and treatment effectiveness. We addressed variability using three climate scenarios and multiple BGI implementation scenarios, capturing a wide range of outcomes. Background concentrations and ingested volumes were modeled with gamma distributions, varying over time to reflect inherent variability and provide a fuller risk assessment. However, QMRA risk estimates depend heavily on dose–response relationships, and common indicators like *E. coli* and enterococci may not always accurately represent specific pathogen risks. Their presence may not correlate with harmful pathogens due to variations in environmental persistence, dilution effects, and differences in microbial characteristics.[120–122] Extrapolating *E. coli* or enterococci concentrations to estimate pathogen levels can, therefore, introduce further uncertainty. To enhance the accuracy of health risk assessments in this study, we directly integrate *Cryptosporidium* and *Giardia* into the PCSWMM model, as detailed in section 2.2. We also conducted a simple linear sensitivity analysis by varying the background concentration in river (C_0) and the pathogen concentration from the CSO events by ±50% to evaluate the impact on infection risk for *Giardia* and *Cryptosporidium* we found out that the dominant source of infection risk differs between pathogens. *Giardia* infection risk is mainly driven by CSO discharges due to their high concentrations, while *Cryptosporidium* risk transitions from CSO to background sources as BGI mitigates CSO flows (details in SI S9).

4.3 Future research

The high-resolution precipitation time series for the hydraulic and hydrologic model were disaggregated from climate model data using a cascade model with stationary parameters. Ebers, Schröter[102] introduced a cascade model with temperature-dependent parameters that produces more intense future precipitation events. Future research should incorporate this non-stationary approach and combine it with spatial disaggregation to better capture climate variable correlations.

The method is developed for a specific pathogen group (protozoa), which restricts the scope of the risk assessment. As part of the QMRA for recreational waters, the US Environmental Protection Agency (EPA) selected eight reference pathogens.[123] These pathogens were chosen due to their involvement in many non-foodborne waterborne illnesses in the United States, their representativeness

regarding the behavior and transport of other waterborne pathogens of concern, and their confirmed presence in recreational waters as well as human and animal excreta.[123] Expanding the method to include multiple pathogen groups would provide a more comprehensive assessment of microbiological water quality risks and improve the robustness of the model. *Norovirus* is one of the most common viral causes of both outbreaks and sporadic cases of gastroenteritis and represents a predominant health risk in recreational waters.[42,124,125] Its presence—and the impact of BGI implementation on its mitigation—could be assessed using the same methodology developed in this study, leveraging *E. coli* outputs from PCSWMM modelling. *E. coli* is typically found at higher concentrations than *Norovirus* in both sewage and environmental waters.[126–128] In untreated sewage effluent, *E. coli* levels can be nearly nine times greater than those of *Norovirus*. In environmental waters, this ratio decreases, ranging from approximately 1.2 to 1.9 depending on salinity, as *E. coli* degrades more rapidly under saline conditions. These ratios can serve as conservative conversion factors for estimating *Norovirus* concentrations—and the associated health risks—when only *E. coli* data are available. In this study we decided to concentrate on *Cryptosporidium* and *Giardia*, since they are protozoa that significantly contribute to waterborne disease outbreaks,[71] and also because we had data on their background concentrations in the river, allowing us to estimate these with a Gamma distribution and include them in our QMRA.

5 Conclusions

The novelty of this research lies in validating that BGI can serve as an effective mitigation measure for the public health challenges posed by the increased occurrence of CSOs under climate change. The study demonstrates the integration of BGI scenarios (0–50% of impervious surfaces) into a coupled discharge-based hydrodynamic and QMRA framework over a 30 year simulation period, providing a probabilistic, temporally explicit evaluation of infection risks in urban recreational waters. Our results show that even small BGI implementations ($\approx$3%) can achieve reductions in infection probability comparable to large storage interventions (28 000 m^3), offering a cost-effective alternative for urban water management. This integrated approach not only supports evidence-based risk assessment but also provides a practical decision-support tool for planners and policymakers to design and prioritize CSO mitigation strategies, maximize public health benefits, and enhance urban resilience under future climate conditions. Investing in measures to prevent CSOs is essential for enhancing sustainable recreational water safety. Future research can build on this approach by applying it to emerging pathogens and contaminants, as well as incorporating comprehensive cost–benefit analyses to compare various CSO reduction strategies and include different BGI types, *e.g.* as proposed for the sponge-city concept. Furthermore, studies could refine resilience

frameworks to develop targeted BGI implementation scenarios that strengthen urban resilience and public health protection. This includes adapting planning-support tools to strategically place BGI, maximizing their effectiveness in reducing overflows, improving stormwater management, and communicating their multiple functions and benefits.

Author contributions

J. Petrucci: writing – review & editing, writing – original draft, visualization, software, methodology, investigation, formal analysis, data curation, conceptualization. J. Derx: writing – review & editing, supervision, resources, project administration, conceptualization. R. Sommer: writing – review & editing, supervision, resources, project administration, conceptualization. J. F. Schijven: writing – review & editing, resources. H. Müller-Thomy: writing – review & editing, resources. S. Dorner: writing – review & editing, supervision, resources, project administration, conceptualization. J. Jalbert: writing – review & editing, supervision, resources, project administration, funding acquisition, conceptualization. F. Bichai: writing – review & editing, supervision, resources, project administration, funding acquisition, conceptualization.

Conflicts of interest

The authors declare that they have no known competing financial interests or personal relationships that could have appeared to influence the work reported in this paper.

Data availability

The original ÖKS15 precipitation dataset used in this study is publicly available at the Geosphere data repository: *ÖKS15 – Klimaszenarien für Österreich: Endbericht – Daten/Data* (dataset), 2018, https://doi.org/10.60669/wgxm-4927.

Due to the large size of the disaggregated high-resolution precipitation time series generated in this study, these derived data are not publicly deposited. However, they are available from the authors upon reasonable request. To request the data, please contact H. Müller-Thomy (h.mueller-thomy@tu-braunschweig.de). The Fortran code used for precipitation disaggregation is also available from the authors upon request.

The hydrological model (HBV) was implemented using the publicly available R package *TUWmodel*: J. Parajka, A. Viglione and G. Blöschl, 2013, CRAN R package **TUWmodel**, https://cran.r-project.org/package=TUWmodel. The related methodological reference is: Parajka, J., Merz, R., & Blöschl, G., *Uncertainty and multiple objective calibration in regional water balance modelling: case study in 320 Austrian catchments. Hydrological Processes*, 2007, 21(4), 435–446. https://doi.org/10.1002/hyp.6253.

Supplementary information (SI): background information for this work, including summaries of the climate scenarios used (S1), the PCSWMM urban drainage model setup (S2),

and bioretention cell modelling based on literature parameters (S3). Also presented are observed river water microbial concentrations and fitted distributions (S4), the HBV-based rainfall-runoff model structure (S5), and additional results on CSO event frequency under multiple climate scenarios, planning horizons, and BGI implementation levels (S6). Further sections report simulated seasonal microorganism concentrations (S7), representative July time-series of Giardia infection risk and CSO flow (S8), and a linear sensitivity analysis evaluating the influence of background and CSO-derived microbial loads on infection risk (S9). See DOI: https://doi.org/10.1039/d5ew00706b.

Acknowledgements

References

1 P. Joshi, J. P. Leitão, M. Maurera and P. M. Bach, Not all SuDS are created equal: Impact of different approaches on combined sewer overflows, *Water Res.*, 2020, **191**, 116780.

2 A.-S. Madoux-Humery, S. Dorner, S. Sauve, K. Aboulfadl, M. Galarneau and P. Servais, *et al.* Temporal variability of combined sewer overflow contaminants: Evaluation of wastewater micropollutants as tracers of fecal contamination, *Water Res.*, 2013, **47**, 4370–4382.

3 H. T. Olds, S. R. Corsi, D. K. Dila, K. M. Halmo, M. J. Bootsma and S. L. McLellan, High levels of sewage contamination released from urban areas after storm events: A quantitative survey with sewage specific bacterial indicators, *PLoS Med.*, 2018, **15**(7), e1002614.

4 A. Miller, S. Ebelt and K. Levy, Combined Sewer Overflows and Gastrointestinal Illness in Atlanta, 2002–2013: Evaluating the Impact of Infrastructure Improvements, *Environ. Health Perspect.*, 2022, **130**(5), 057009.

5 B. M. Haley, Y. Sun, J. S. Jagai, J. H. Leibler, R. Fulweiler and J. Ashmore, *et al.* Association between Combined Sewer Overflow Events and Gastrointestinal Illness in Massachusetts

Municipalities with and without River-Sourced Drinking Water, 2014–2019, *Environ. Health Perspect.*, 2024, **132**(5), 057008.

6   USEPA, *Report to Congress: impacts and control of CSOs and SSOs*, Washington, DC, USA, 2004.

7   K. Pongmala, L. Autixier, A.-S. Madoux-Humery, M. Fuamba, M. Galarneau and S. Sauvé, *et al.* Modelling total suspended solids, E. coli and carbamazepine, a tracer of wastewater contamination from combined sewer overflows, *J. Hydrol.*, 2015, **531**, 830–839.

8   E. Quaranta, S. Fuchs, H. Jan Liefting, A. Schellart and A. Pistocchi, A hydrological model to estimate pollution from combined sewer overflows at the regional scale: Application to Europe, *J. Hydrol. Reg. Stud.*, 2022, **41**, 101080.

9   J. Derx, H. Müller-Thomy, H. S. Kılıç, S. Cervero-Arago, R. Linke and G. Lindner, *et al.* A probabilistic-deterministic approach for assessing climate change effects on infection risks downstream of sewage emissions from CSOs, *Water Res.*, 2023, **247**, 120746.

10 J. A. Patz, S. J. Vavrus, C. K. Uejio and S. L. McLellan, Climate Change and Waterborne Disease Risk in the Great Lakes Region of the U.S, *Am. J. Prev. Med.*, 2008, **35**(5), 451–458.

11 J. Petrucci, J. Jalbert, S. Dorner, N. McQuaid and F. Bichai, Strategic prioritization of sewersheds to mitigate combined sewer overflows under climate change, *Environ. Challenges*, 2025, **18**, 101088.

12 B. Leveque, J.-B. Burnet, S. Dorner and F. Bichai, Impact of climate change on the vulnerability of drinking water intakes in a northern region, *Sustainable Cities and Society*, 2021, **66**, 102656.

13 A. Sterk, H. de Man, J. F. Schijven, T. de Nijs and A. M. de Roda Husman, Climate change impact on infection risks during bathing downstream of sewage emissions from CSOs or WWTPs, *Water Res.*, 2016, **105**, 11–21.

14 USEPA, *A Screening Assessment of the Potential Impacts of Climate Change on Combined Sewer Overflow (CSO) Mitigation In the Great Lakes and New England Regions*, 2008.

15 I. Jalliffier-Verne, R. Leconte, U. Huaringa-Alvarez, A.-S. Madoux-Humery, M. Galarneau and P. Pierre Servais, *et al.* Impacts of global change on the concentrations and dilution of combined sewer overflows in a drinking water source, *Sci. Total Environ.*, 2015, **508**, 462–476.

16 K. Schroeder, M. Riechel, A. Matzinger, P. Rouault, H. Sonnenberg and E. Pawlowsky-Reusing, *et al.* Evaluation of effectiveness of combined sewer overflow control measures by operational data, *Water Sci. Technol.*, 2011, **63**(2), 325–330.

17 S. Even, J.-M. Mouchel, P. Servais, N. Flipo, M. Poulin and S. Blanc, *et al.* Modelling the impacts of Combined Sewer Overflows on the river Seine water quality, *Sci. Total Environ.*, 2007, **375**(1), 140–151.

18 P. Willems and J. Olsson, *Impacts of climate change on rainfall extremes and urban drainage systems*, IWA publishing, 2012.

19 I. E. Schneider, Urban Water Recreation: Experiences, Place Meanings, and Future Issues, in *The Water Environment of Cities*, ed. L. A. Baker, Springer US, Boston, MA, 2009, pp. 125–140.

20 D. García-León, P. Masselot, M. N. Mistry, A. Gasparrini, C. Motta and L. Feyen, *et al.* Temperature-related mortality burden and projected change in 1368 European regions: a modelling study, *Lancet Public Health*, 2024, **9**(9), e644–e653.

21 S. Merte, Estimating heat wave-related mortality in Europe using singular spectrum analysis, *Clim. Change*, 2017, **142**(3), 321–330.

22 Z. S. Venter, N. H. Krog and D. N. Barton, Linking green infrastructure to urban heat and human health risk mitigation in Oslo, Norway, *Sci. Total Environ.*, 2020, **709**, 136193.

23 F. Marando, E. Salvatori, A. Sebastiani, L. Fusaro and F. Manes, Regulating Ecosystem Services and Green Infrastructure: assessment of Urban Heat Island effect mitigation in the municipality of Rome, Italy, *Ecol. Modell.*, 2019, **392**, 92–102.

24 H. Zhou, Q. Wang, N. Zhu, Y. Li, J. Li and L. Zhou, *et al.* Optimization Methods of Urban Green Space Layout on Tropical Islands to Control Heat Island Effects, *Energies*, 2023, **16**(1), 368.

25 M. Sadeghi, T. Chaston, I. Hanigan, R. de Dear, M. Santamouris and B. Jalaludin, *et al.* The health benefits of greening strategies to cool urban environments – A heat health impact method, *Build. Environ.*, 2022, **207**, 108546.

26 S. Wuijts, M. de Vries, W. Zijlema, J. Hin, L. R. Elliott and L. D.-V. Breemen, *et al.* The health potential of urban water: Future scenarios on local risks and opportunities, *Cities*, 2022, **125**, 103639.

27 M. P. White, L. R. Elliott, M. Gascon, B. Roberts and L. E. Fleming, Blue space, health and well-being: A narrative overview and synthesis of potential benefits, *Environ. Res.*, 2020, **191**, 110169.

28 World Health Organization, *Urban green spaces and health. A review of evidence*, 2016.

29 M. Gascon, W. Zijlema, C. Vert, M. P. White and M. J. Nieuwenhuijsen, Outdoor blue spaces, human health and well-being: A systematic review of quantitative studies, *Int. J. Hyg. Environ. Health*, 2017, **220**(8), 1207–1221.

30 USEPA, *What is Green Infrastructure?*, 2021, [Available from: https://www.epa.gov/green-infrastructure/what-green-infrastructure#rainwaterharvesting].

31 MELCC, *Guide de gestion des eaux pluviales. Québec Gd*, Gouvernement du Québec, Québec, Canada, 2014, p. 86.

32 L. Autixier, A. Mailhot, S. Bolduc, A.-S. Madoux-Humery, M. Galarneau and M. Prévost, *et al.* Evaluating rain gardens as a method to reduce the impact of sewer overflows in sources of drinking water, *Sci. Total Environ.*, 2014, **499**, 238–247.

33 USEPA, *Greening CSO Plans: Planning and Modeling Green Infrastructure for Combined Sewer Overflow (CSO) Control*, 2014, Report No.: 832-R-14-001.

34 C. Li, C. Peng, P.-C. Chiang, Y. Cai, X. Wang and Z. Yang, Mechanisms and applications of green infrastructure practices for stormwater control: A review, *J. Hydrol.*, 2019, **568**, 626–637.

35 P. Anquez and A. Herlem, *Les îlots de chaleur dans la région métropolitaine de Montréal: causes, impacts et solutions*

UQAM, Chaire de responsabilité sociale et de développement durable, 2011.

36 W.-L. Tsai, L. Yngve, Y. Zhou, K. M. M. Beyer, A. Bersch and K. M. Malecki, *et al.* Street-level neighborhood greenery linked to active transportation: A case study in Milwaukee and Green Bay, WI, USA, *Landsc. Urban Plann.*, 2019, **191**, 103619.

37 D. Dagenais, I. Thomas and S. Paquette, Siting green stormwater infrastructure in a neighbourhood to maximise secondary benefits: lessons learned from a pilot project, *Landsc. Res.*, 2017, **42**(2), 195–210.

38 B. Rayfiel, A. Paquette, A. Gonzalez, C. Messier, D. Dagenais and J. Dupras, *et al.*, *Les infrastructures vertes: Un outil d'adaptation aux changements climatiques pour le Grand Montréal*, 2015.

39 S. Wuijts, L. Friederichs, J. A. Hin, F. M. Schets, H. F. M. W. Van Rijswick and P. P. J. Driessen, Governance conditions to overcome the challenges of realizing safe urban bathing water sites, *International Journal of Water Resources Development*, 2022, **38**(4), 554–578.

40 A. O. Sojobi and T. Zayed, Impact of sewer overflow on public health: A comprehensive scientometric analysis and systematic review, *Environ. Res.*, 2022, **203**, 111609.

41 F. E. Eregno, I. Tryland, T. Tjomsland, M. Myrmel, L. Robertson and A. Heistad, Quantitative microbial risk assessment combined with hydrodynamic modelling to estimate the public health risk associated with bathing after rainfall events, *Sci. Total Environ.*, 2016, **548–549**, 270–279.

42 G. B. McBride, R. Stott, W. Miller, D. Bambic and S. Wuertz, Discharge-based QMRA for estimation of public health risks from exposure to stormwater-borne pathogens in recreational waters in the United States, *Water Res.*, 2013, **47**(14), 5282–5297.

43 S. Kozak, S. Petterson, T. McAlister, I. Jennison, S. Bagraith and A. Roiko, Utility of QMRA to compare health risks associated with alternative urban sewer overflow management strategies, *J. Environ. Manage.*, 2020, **262**, 110309.

44 C. Timm, S. Luther, L. Jurzik, I. A. Hamza and T. Kistemann, Applying QMRA and DALY to assess health risks from river bathing, *Int. J. Hyg. Environ. Health*, 2016, **219**(7 Pt B), 681–692.

45 I. Oluk, Quantitative Microbial Risk Assessment (QMRA) For Urban Stormwater Reuse After Treatment Through A Bioretention System, *Master's Thesis (MS)*, University of Kentucky, 2023.

46 D. W. B. Rosa, C. V. P. S. Hot, I. T. Gomes, D. F. Ventura, T. F. G. Silva and J. Chong, *et al.* Water quality benefits of implementing Green and Blue Infrastructure in a peri-urban catchment – Case study of a Brazilian metropolis, *J. Cleaner Prod.*, 2024, **478**, 143943.

47 B. Chimani, C. Matulla, J. Eitzinger, T. Gorgas-Schellander, J. Hiebl and M. Hofstätter, *et al.*, *Guideline zur Nutzung der OeKS15-Klimawandelsimulationen sowie der entsprechenden gegitterten Beobachtungsdatensätze*, CCCA Data Centre, 2018, vol. 450.

48 E. Lapierre, *Portrait des infrastructures vertes et des ouvrages phytotechnologiques dans l'agglomération de Montréal*, Pour Fondation Espace pour la vie, 2018.

49 CCCA, *Climate Change Centre Austria*, 2020, [Available from: https://ccca.ac.at/startseite].

50 K. E. Taylor, R. J. Stouffer and G. A. Meehl, An overview of CMIP5 and the experiment design, *Bull. Am. Meteorol. Soc.*, 2012, **93**(4), 485–498.

51 H. Müller and U. Haberlandt, Temporal rainfall disaggregation with a cascade model: from single-station disaggregation to spatial rainfall, *J. Hydrol. Eng.*, 2015, **20**(11), 04015026.

52 Improving the autocorrelation in disaggregated time series for urban hydrological applications, in *Rainfall Monitoring, Modelling and Forecasting in Urban Environment UrbanRain18: 11th International Workshop on Precipitation in Urban Areas Conference Proceeding*, ed. H. Müller-Thomy, Institute of Environmental Engineering, ETH Zurich, 2019.

53 H. Müller-Thomy, Temporal rainfall disaggregation using a micro-canonical cascade model: possibilities to improve the autocorrelation, *Hydrol. Earth Syst. Sci.*, 2020, **24**(1), 169–188.

54 H. Müller and U. Haberlandt, Temporal rainfall disaggregation using a multiplicative cascade model for spatial application in urban hydrology, *J. Hydrol.*, 2018, **556**, 847–864.

55 D. Kim and F. Olivera, Relative importance of the different rainfall statistics in the calibration of stochastic rainfall generation models, *J. Hydrol. Eng.*, 2012, **17**(3), 368–376.

56 G. Blöschl, C. Reszler and J. Komma, A spatially distributed flash flood forecasting model, *Environ. Model. Softw.*, 2008, **23**(4), 464–478.

57 L. A. Rossman, *Storm Water Management Model Reference Manual*, 2017.

58 L. A. Rossman and W. C. Huber, *Storm Water Management Model Reference Manual Volume III – Water Quality*, 2016.

59 Computational Hydraulics International (CHI), PCSWMM 2024 [EPA STORM WATER MANAGEMENT MODEL – VERSION 5.2 (Build 5.2.4)]: [Available from: https://www.pcswmm.com/Downloads/PCSWMM].

60 W. F. Hunt, A. R. Jarrett, J. T. Smith and L. J. Sharkey, Evaluating Bioretention Hydrology and Nutrient Removal at Three Field Sites in North Carolina, *J. Irrig. Drain. Eng.*, 2006, **132**(6), 600–608.

61 W. F. Hunt, J. T. Smith, S. J. Jadlocki, J. M. Hathaway and P. R. Eubanks, Pollutant Removal and Peak Flow Mitigation by a Bioretention Cell in Urban Charlotte, N.C, *J. Environ. Eng.*, 2008, **134**(5), 403–408.

62 M. Kõiv-Vainik, K. Kill, M. Espenberg, E. Uuemaa, A. Teemusk and M. Maddison, *et al.* Urban stormwater retention capacity of nature-based solutions at different climatic conditions, *Nat.-Based Solution*, 2022, **2**, 100038.

63 G. Gougeon, O. Bouattour, E. Formankova, J. St-Laurent, S. Doucet and S. Dorner, *et al.* Impact of bioretention cells in cities with a cold climate: modeling snow management based on a case study, *Blue-Green Syst.*, 2023, **5**(1), 1–17.

64 O. Bouattour, Caractérisation de l'impact de cellules de biorétention sur la qualité et la quantité des eaux pluviales à Trois-Rivières, *Master's thesis (MASc)*, Québec PolyPublie: Polytechnique Montréal, 2021.

65 J. Furchtlehner, D. Lehner and L. Lička, Sustainable Streetscapes: Design Approaches and Examples of Viennese Practice, *Sustainability*, 2022, **14**(2), 961.

66 Avizo, *Les systèmes de biorétention: des OGEP pour les milieux urbains*, 2022, [Available from: https://www.avizo.ca/2022/02/01/les-systemes-de-bioretention-des-ogep-pour-les-milieux-urbains/#:~:text=Une%20norme%20de%20conception%20des%20syst].

67 F. M. Schets, J. F. Schijven and A. M. de Roda Husman, Exposure assessment for swimmers in bathing waters and swimming pools, *Water Res.*, 2011, **45**(7), 2392–2400.

68 J. Schijven, J. Derx, A. M. de Roda Husman, A. P. Blaschke and A. H. Farnleitner, QMRAcatch: Microbial Quality Simulation of Water Resources including Infection Risk Assessment, *J. Environ. Qual.*, 2015, **44**(5), 1491–1502.

69 Gouvernement du Canada, *Canadian recreational water quality guidelines – Indicators of fecal contamination: E. coli and enterococci in recreational waters*, 2023, [Available from: https://www.canada.ca/en/health-canada/services/publications/healthy-living/recreational-water-quality-guidelines-indicators-fecal-contamination/e-coli-enterococci.html].

70 World Health Organization, *Guidelines on recreational water quality. Volume 1: coastal and fresh waters*, 2021.

71 Health Canada, *Guidelines for Canadian Drinking Water Quality: Guideline Technical Document—Enteric Protozoa: Giardia and Cryptosporidium. Ottawa, Ontario: Water and Air Quality Bureau, Healthy Environments and Consumer Safety Branch, Health Canada*, 2019, Contract No.: Catalogue No. H144-13/10-2018E-PDF.

72 Gouvernement du Canada, *Recommandations pour la qualité de l'eau potable au Canada-Protozoaires entériques: Giardia et Cryptosporidium*, 2012.

73 A. Efstratiou, J. E. Ongerth and P. Karanis, Waterborne transmission of protozoan parasites: Review of worldwide outbreaks – An update 2011–2016, *Water Res.*, 2017, **114**, 14–22.

74 C. Júlio, C. Sá, I. Ferreira, S. Martins, M. Oleastro and H. Ângelo, *et al.* Waterborne transmission of Giardia and Cryptosporidium at river beaches in Southern Europe (Portugal), *J. Water Health*, 2012, **10**(3), 484–496.

75 J. J. Gannon and M. K. Busse, E. coli and enterococci levels in urban stormwater, river water and chlorinated treatment plant effluent, *Water Res.*, 1989, **23**(9), 1167–1176.

76 K. Borel, R. Karthikeyan, T. A. Berthold and K. Wagner, Estimating E. coli and Enterococcus loads in a coastal Texas watershed, *Texas Water Journal*, 2015, **6**(1), 33–44.

77 P. F. M. Teunis and A. H. Havelaar, The Beta Poisson Dose-Response Model Is Not a Single-Hit Model, *Risk Anal.*, 2000, **20**(4), 513–520.

78 S. Regli, J. B. Rose, C. N. Haas and C. P. Gerba, Modeling the Risk From Giardia and Viruses in Drinking Water, *J. AWWA*, 1991, **83**(11), 76–84.

79 S. Moghadas, G. Leonhardt, J. Marsalek and M. Viklander, Modeling Urban Runoff from Rain-on-Snow Events with the U.S. EPA SWMM Model for Current and Future Climate Scenarios, *J. Cold Reg. Eng.*, 2018, **32**(1), 04017021.

80 S. Moghadas, A.-M. Gustafsson, P. Viklander, J. Marsalek and M. Viklander, Laboratory study of infiltration into two frozen engineered (sandy) soils recommended for bioretention, *Hydrol. Processes*, 2016, **30**(8), 1251–1264.

81 A. Montserrat, O. Gutierrez, M. Poch and L. Corominas, Field validation of a new low-cost method for determining occurrence and duration of combined sewer overflows, *Sci. Total Environ.*, 2013, **463–464**, 904–912.

82 W. Q. Betancourt and J. B. Rose, Drinking water treatment processes for removal of Cryptosporidium and Giardia, *Vet. Parasitol.*, 2004, **126**(1), 219–234.

83 B. A. Norton, A. M. Coutts, S. J. Livesley, R. J. Harris, A. M. Hunter and N. S. G. Williams, Planning for cooler cities: A framework to prioritise green infrastructure to mitigate high temperatures in urban landscapes, *Landsc. Urban Plann.*, 2015, **134**, 127–138.

84 C. Coutts and M. Hahn, Green Infrastructure, Ecosystem Services, and Human Health, *Int. J. Environ. Res. Public Health*, 2015, **12**(8), 9768–9798.

85 J. Passerat, N. K. Ouattara, J.-M. Mouchel, R. Vincent and P. Servais, Impact of an intense combined sewer overflow event on the microbiological water quality of the Seine River, *Water Res.*, 2011, **45**(2), 893–903.

86 A.-S. Madoux-Humery, S. M. Dorner, S. Sauvé, K. Aboulfadl, M. Galarneau and P. Servais, *et al.* Temporal analysis of E. coli, TSS and wastewater micropollutant loads from combined sewer overflows: implications for management, *Environ. Sci.: Processes Impacts*, 2015, **17**(5), 965–974.

87 M. A. Launay, U. Dittmer and H. Steinmetz, Organic micropollutants discharged by combined sewer overflows – Characterisation of pollutant sources and stormwater-related processes, *Water Res.*, 2016, **104**, 82–92.

88 P. Phillips, A. Chalmers, J. Gray, D. Kolpin, W. Foreman and G. Wall, Combined sewer overflows: an environmental source of hormones and wastewater micropollutants, *Environ. Sci. Technol.*, 2012, **46**(10), 5336–5343.

89 A. Botturi, E. G. Ozbayram, K. Tondera, N. I. Gilbert, P. Rouault and N. Caradot, *et al.* Combined sewer overflows: A critical review on best practice and innovative solutions to mitigate impacts on environment and human health, *Crit. Rev. Environ. Sci. Technol.*, 2021, **51**(15), 1585–1618.

90 E. Quaranta, S. Fuchs, H. J. Liefting, A. Schellart and A. Pistocchi, Costs and benefits of combined sewer overflow management strategies at the European scale, *J. Environ. Manage.*, 2022, **318**, 115629.

91 E. Donovan, K. Unice, J. D. Roberts, M. Harris and B. Finley, Risk of gastrointestinal disease associated with exposure to pathogens in the water of the Lower Passaic River, *Appl. Environ. Microbiol.*, 2008, **74**(4), 994–1003.

92 W. C. Lucas and D. J. Sample, Reducing combined sewer overflows by using outlet controls for Green Stormwater Infrastructure: Case study in Richmond, Virginia, *J. Hydrol.*, 2015, **520**, 473–488.

93 T. Lucke and P. W. B. Nichols, The pollution removal and stormwater reduction performance of street-side

bioretention basins after ten years in operation, *Sci. Total Environ.*, 2015, **536**, 784–792.

94 G. B. Cavadini, M. Rodriguez, T. Nguyen and L. M. Cook, Can blue–green infrastructure counteract the effects of climate change on combined sewer overflows? Study of a swiss catchment, *Environ. Res. Lett.*, 2024, **19**(9), 094025.

95 M. Weathers, J. M. Hathaway, R. A. Tirpak and A. Khojandi, Evaluating the impact of climate change on future bioretention performance across the contiguous United States, *J. Hydrol.*, 2023, **616**, 128771.

96 Z. Zahmatkesh, S. J. Burian, M. Karamouz, H. Tavakol-Davani and E. Goharian, Low-Impact Development Practices to Mitigate Climate Change Effects on Urban Stormwater Runoff: Case Study of New York City, *J. Irrig. Drain. Eng.*, 2015, **141**(1), 04014043.

97 S. N. Mugume and L. P. Nakyanzi, Evaluation of effectiveness of Blue-Green Infrastructure for reduction of pluvial flooding under climate change and internal system failure conditions, *Blue-Green Syst.*, 2024, **6**(2), 264–292.

98 T. Benoit, J.-L. Martel, É. Bilodeau, F. Brissette, A. Charron and D. Brulé, *et al.* Limits of Blue and Green Infrastructures to Adapt Actual Urban Drainage Systems to the Impact of Climate Change, *J. Irrig. Drain. Eng.*, 2025, **151**(2), 04025003.

99 K. Haslinger, K. Breinl, L. Pavlin, G. Pistotnik, M. Bertola and M. Olefs, *et al.* Increasing hourly heavy rainfall in Austria reflected in flood changes, *Nature*, 2025, **639**(8055), 667–672.

100 S. Spraakman, J.-L. Martel and J. Drake, How much water can bioretention retain, and where does it go?, *Blue-Green Syst.*, 2022, **4**(2), 89–107.

101 J. Kyselý and R. Beranová, Climate-change effects on extreme precipitation in central Europe: uncertainties of scenarios based on regional climate models, *Theor. Appl. Climatol.*, 2009, **95**(3), 361–374.

102 N. Ebers, K. Schröter and H. Müller-Thomy, Estimation of future rainfall extreme values by temperature-dependent disaggregation of climate model data, *Nat. Hazards Earth Syst. Sci.*, 2024, **24**(6), 2025–2043.

103 R. A. Tirpak, J. M. Hathaway, A. Khojandi, M. Weathers and T. H. Epps, Building resiliency to climate change uncertainty through bioretention design modifications, *J. Environ. Manage.*, 2021, **287**, 112300.

104 M. B. de Macedo, M. N. Gomes Jr, V. Jochelavicius, T. R. P. de Oliveira and E. M. Mendiondo, Modular Design of Bioretention Systems for Sustainable Stormwater Management under Drivers of Urbanization and Climate Change, *Sustainability*, 2022, **14**(11), 6799.

105 P. Persaud, A. Akin, B. Kerkez, D. McCarthy and J. Hathaway, Real time control schemes for improving water quality from bioretention cells, *Blue-Green Syst.*, 2019, **1**(1), 55–71.

106 P. Shen, A. Deletic, K. Bratieres and D. T. McCarthy, Real time control of biofilters delivers stormwater suitable for harvesting and reuse, *Water Res.*, 2020, **169**, 115257.

107 L. Krauss and M. A. Rippy, Plant adaptive strategy influences hydrologic services provisioning by stormwater bioretention, *Ecol. Eng.*, 2024, **198**, 107148.

108 S. H. Ghodsi, Z. Zahmatkesh, E. Goharian, R. Kerachian and Z. Zhu, Optimal design of low impact development practices in response to climate change, *J. Hydrol.*, 2020, **580**, 124266.

109 D. Dagenais, S. Paquette, M. Fuamba, E. J. Servier, A. Spector and L. Besson, *et al.*, Participatory Design of a Decision Aid Tool Integrating Social Aspects for the Implementation of at Source Vegetated Best Management Practices (SVBMPs) at the Neighbourhood Level, *Novatech 2013 – 8ème Conférence internationale sur les techniques et stratégies durables pour la gestion des eaux urbaines par temps de pluie*, Lyon, France, 2013.

110 M. Kuller, P. M. Bach, S. Roberts, D. Browne and A. Deletic, A planning-support tool for spatial suitability assessment of green urban stormwater infrastructure, *Sci. Total Environ.*, 2019, **686**, 856–868.

111 S. Lacroix, M. Kuller, G. Gougeon, J. Petrucci, F. Lemieux-Chalifour and A. Rioux, *et al.* Can we stop reinventing the wheel in blue-green infrastructure planning? Using value-focused thinking to enable transferability of a multicriteria planning support system, *Landsc. Urban Plann.*, 2024, **252**, 105188.

112 S. B. Yaagoubi, Évaluation de l'efficacité des infrastructures vertes, et de leur implantation stratégique, dans la lutte contre le ruissellement urbain et les surverses, *Master's thesis (MASc)*, Polytechnique Montréal, Montréal, 2025.

113 J. Petrucci, S. B. Yaagoubi, S. Dorner, J. Jalbert and F. Bichai, *Assessing the impact of strategic implementation of blue-green infrastructure on urban resilience*, 2025.

114 G. B. Cavadini, M. Rodriguez and L. M. Cook, Connecting blue-green infrastructure elements to reduce combined sewer overflows, *J. Environ. Manage.*, 2024, **365**, 121465.

115 ClimateData, *CMIP6 Frequently Asked Questions*, 2025, [Available from: https://climatedata.ca/?].

116 D. Ma, Z. Bai, Y.-P. Xu, H. Gu and C. Gao, Assessing streamflow and sediment responses to future climate change over the Upper Mekong River Basin: A comparison between CMIP5 and CMIP6 models, *J. Hydrol. Reg. Stud.*, 2024, **52**, 101685.

117 S.-C. Bourdeau-Goulet and E. Hassanzadeh, Comparisons Between CMIP5 and CMIP6 Models: Simulations of Climate Indices Influencing Food Security, Infrastructure Resilience, and Human Health in Canada, *Earth's Future*, 2021, **9**(5), e2021EF001995.

118 K. A. Hamilton, J. Ciol Harrison, J. Mitchell, M. Weir, M. Verhougstraete and C. N. Haas, *et al.* Research gaps and priorities for quantitative microbial risk assessment (QMRA), *Risk Anal.*, 2024, **44**(11), 2521–2536.

119 D. de Brito Cruz, P. J. Schmidt and M. B. Emelko, Drinking water QMRA and decision-making: Sensitivity of risk to common independence assumptions about model inputs, *Water Res.*, 2024, **259**, 121877.

120 V. J. Harwood, C. Staley, B. D. Badgley, K. Borges and A. Korajkic, Microbial source tracking markers for detection of fecal contamination in environmental waters: relationships between pathogens and human health outcomes, *FEMS Microbiol. Rev.*, 2014, **38**(1), 1–40.

121 P. Payment and A. Locas, Pathogens in water: value and limits of correlation with microbial indicators, *Ground Water*, 2011, **49**(1), 4–11.

122 K. Skiendzielewski, T. Burch, J. Stokdyk, S. McGinnis, S. McLoughlin and A. Firnstahl, *et al.* Two risk assessments: Evaluating the use of indicator HF183 Bacteroides versus pathogen measurements for modelling recreational illness risks in an urban watershed, *Water Res.*, 2024, **259**, 121852.

123 USEPA, *Quantitative microbial risk assessment to estimate illness in freshwater impacted by agricultural animal sources of fecal contamination*, United States Environmental Protection Agency, Washington, DC, 2010.

124 G. La Rosa, M. Pourshaban, M. Iaconelli and M. Muscillo, Recreational and drinking waters as a source of norovirus gastroenteritis outbreaks: a review and update, *Environ. Biotechnol.*, 2008, **4**(1), 15–24.

125 A. Polkowska, S. Räsänen, H. Al-Hello, M. Bojang, O. Lyytikäinen and J. P. Nuorti, *et al.* An outbreak of Norovirus infections associated with recreational lake water in Western Finland, 2014, *Epidemiol. Infect.*, 2018, **146**(5), 544–550.

126 A. Tiwari, A. Kauppinen, P. Räsänen, J. Salonen, L. Wessels and J. Juntunen, *et al.* Effects of temperature and light exposure on the decay characteristics of fecal indicators, norovirus, and Legionella in mesocosms simulating subarctic river water, *Sci. Total Environ.*, 2023, **859**, 160340.

127 K. Inoue, T. Asami, T. Shibata, H. Furumai and H. Katayama, Spatial and temporal profiles of enteric viruses in the coastal waters of Tokyo Bay during and after a series of rainfall events, *Sci. Total Environ.*, 2020, **727**, 138502.

128 W. J. Kim, S. Managaki, H. Furumai and F. Nakajima, Diurnal fluctuation of indicator microorganisms and intestinal viruses in combined sewer system, *Water Sci. Technol.*, 2009, **60**(11), 2791–2801.